Appl. Phys. A (2015) 119:1069–1074
DOI 10.1007/s00339-015-9069-4

Applied Physics A
Materials Science & Processing

Carbon coated to improve the electrochemical properties of $LiMn_2O_4$ cathode material synthesized by the novel acetone hydrothermal method

Qianqian Jiang · Lei Xu · Zhaoling Ma · Han Zhang

Received: 9 December 2014 / Accepted: 20 February 2015 / Published online: 27 February 2015

Abstract Spinel $LiMn_2O_4$ particle is successfully synthesized by the acetone hydrothermal method without further sintered at high temperature. The electrochemical performances of $LiMn_2O_4$ at room temperature are improved by carbon modification through a post-heat treatment. SEM exhibits that the particles are well distributed and the primary grains are 5 μm in size. TEM indicates that the $LiMn_2O_4$/C is uniformly coated with a carbon layer about 2.0 nm in size. The electrochemical performances show that the pristine sample has an initial discharge capacity of 127.9 mAh g^{-1}, and the capacity decreases to 110.6 mAh g^{-1} with the losses of 14.2 % after 100 cycles. Apparently, the $LiMn_2O_4$/C exhibits an initial capacity with 134.9 mAh g^{-1}, and capacity losses of only 4.3 % after 100 cycles. At a discharge rate of 1 C, it keeps more than 97.18 % of the reversible capacity compared with that at 0.1 C. At the same time, the sample $LiMn_2O_4$/C shows only 5.84 % discharge capacity loss at the elevated temperature. The results show that the $LiMn_2O_4$/C sample with excellent electrochemical performances should attribute to the carbon layer avoiding the core material direct contact with the acidic electrolyte and suppression of Mn^+ dissolution into electrolyte.

Q. Jiang (✉) · H. Zhang
College of Photoelectric Engineering, Shenzhen University, Shenzhen 518052, China
e-mail: kaiqian@tju.edu.cn; kaiqian2008@163.com

Q. Jiang · L. Xu · Z. Ma
College of Chemistry and Chemical Engineering, Hunan University, Hunan 410082, China

1 Introduction

Spinel-phase $LiMn_2O_4$ has been considered to be the most promising cathode for lithium-ion batteries owing to its advantages of abundant manganese resources, low cost, ecofriendly in nature, high theoretic capacity and facility of production [1, 2], compared with layered $LiCoO_2$ and $LiNiO_2$ oxides [3–6]. It is well known that the electrochemical performance of a cathode material is greatly associated with the particle properties such as size, morphology and specific surface area. The traditionally synthesized $LiMn_2O_4$ often has large particle size (micrometer level or even larger) and oxygen deficiency, which results in low power density, and it also suffers the drawback of poor cycling stability [7–9] in the meanwhile. Although the traditional method has many disadvantages such as high energy consumption, low efficiency, lack of fine powder and so on, it is easy to be accomplished industrialization and application. On the contrary, liquid-phase methods, such as sol–gel method [10], co-precipitation method [11] and hydrothermal method [12–14], can improve the purity and reduce the particle size of $LiMn_2O_4$, which can reduce the diffusion distance of lithium ion in cathode materials and accelerate extrusion speed to improve the electrochemical performance of materials. However, $LiMn_2O_4$ suffers fast capacity fading during cycling, which is the major obstacle to its commercialization. Although spinel $LiMn_2O_4$ has many advantages, its poor electrical conductivity has been considered a limiting factor for using in high-power applications. Another challenging issue with cathodes made of $LiMn_2O_4$ is that the capacity decays significantly with charge–discharge cycling, which has been a major problem prohibiting $LiMn_2O_4$ from commercial application [15]. So far, several reasons are advanced to explain its poor cycling performance, including structural

instability, Jahn–Teller distortion and Mn dissolution into electrolyte [16–24]. Many scientists and engineers all over the world have made great efforts to improve the cycling performance of $LiMn_2O_4$ at room temperature.

In our recent work, we not only develope the synthesis of $LiMn_2O_4$ via a new hydrothermal route at the relatively low temperature, but also improve the electrochemical performances through carbon layer on the surface of the $LiMn_2O_4$. Compared with other methods, the hydrothermal route as reported in this paper has a lot of merits: low reaction temperature which reduces the cost of the process, the low pressure of autoclave, environmentally friendly and so on. Besides, the effects of carbon layer on the electrochemical performances of $LiMn_2O_4$ at room temperature are investigated. Furthermore, this method has been proved to be a promising treatment for $LiMn_2O_4$ sample. The experiment results show that the $LiMn_2O_4$/C product exhibits excellent electrochemical performances at room temperature compared to the pristine materials.

2 Experimental

The spinel $LiMn_2O_4$ is synthesized by a novel acetone hydrothermal method. Stoichiometric amount of $KMnO_4$ is dissolved in a certain amount of single distilled water, and a certain amount of $LiOH{\cdot}H_2O$ is slowly added into the purple solution with the magnetic stirring. The molar ratio of the Li:Mn is 1:2. After stirring for 20 min, the certain amount of acetone is added into the mixed solution. The solution is transferred into a stainless steel autoclave after homogeneous mixing. At last, the stainless steel autoclaves are seated and heated at 120 °C for 6 h. After being cooled to room temperature, the product is washed several times with deionized water. The obtained powder is subsequently dried at 80 °C for 4 h in air. The obtained samples mixing a measured amount of glucose are sintered at 600 °C for 2 h in a tubular furnace under argon atmosphere.

Structural and phase analysis of the resulting powders is carried out by X-ray diffraction (XRD) (Model D2500v/pc, Rigaku, Japan) with Cu Ka radiation (40 kV, 200 mA), with 2θ in the 10°–80° range. Their morphology and carbon-coating layer of the sample are characterized by the Transmission Electron Microscope (TEM) (100CX-II made by JEOL, Tokyo, Japan). Scanning electron microscope (SEM; Hitachi S-4800, Japan) is applied to observe morphologies of the samples.

At room temperature, the electrochemical characterization is performed using CR2032 coin-type test cells made in the glove box. The electrochemical measurements are taken on a two-electrode testing cell fabricated in this work, using lithium as the counter electrode. The electrolyte consists of 1.0 mol L^{-1} $LiPF_6$ in ethylene carbonate (EC) and dimethyl carbonate (DMC) in a 1:1 (w/w) ratio. Galvanostatic cycling tests of the assembled cells are carried out on an LAND system (made in China) in the voltage range of 3.0–4.3 V (vs Li^+/Li) at various current densities at room temperature in order to estimate the discharge, rate capacity and cycle-life performance.

3 Results and discussion

Figure 1 shows XRD patterns of $LiMn_2O_4$ and $LiMn_2O_4$/C powders. All the intense peaks in the spectrum clearly show single-phase formation of a spinel structure, indicating the two samples without any obvious impurities such as $LiMnO_2$ and MnO_2, which often appear in the $LiMn_2O_4$ product synthesized by the traditional route. Besides, the diffraction peaks at 18.66°, 36.30°, 38.06°, 38.06°, 44.1°, 48.3°, 58.21°, 63.80° and 67.38° are indexed to the spinel $LiMn_2O_4$, which are close to those reported in the JCPDS data (JCPDS No. 35-0782). However, the peaks of the $LiMn_2O_4$ (Fig. 1b) with sintered at 600 °C for 2 h are more narrower and sharper than the pristine $LiMn_2O_4$ (Fig. 1a), which presents a good crystalline degree compared with bare $LiMn_2O_4$. The XRD pattern of the $LiMn_2O_4$/C (Fig. 1b) sample shows an increase in intensity of the peaks with a peak broadening, indicating that the formed carbon can provide a network structure to impede the agitation of the pristine $LiMn_2O_4$. On the other hand, sharp peaks imply the crystallinity of the materials. All the diffraction peaks of the XRD patterns can be indexed to a pure phase-centered cubic which is in good agreement with those reported previously [25, 26], thus demonstrating the high purity and well crystallinity of the as-synthesized spinel $LiMn_2O_4$.

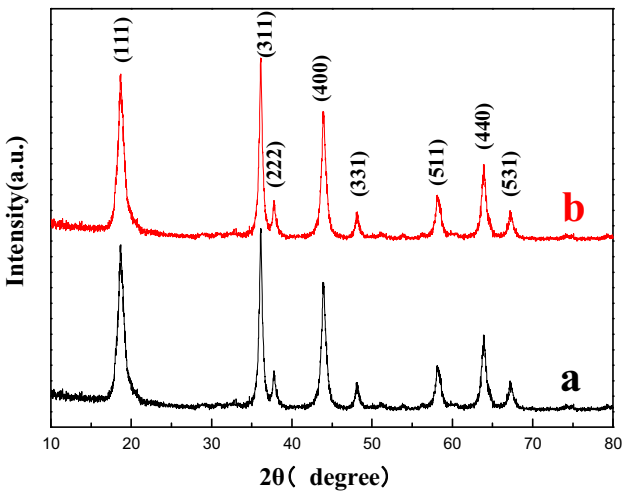

Fig. 1 XRD patterns of $LiMn_2O_4$ and $LiMn_2O_4$/C synthesized in this study

Simultaneously, no obvious peaks corresponding to graphite are found in the XRD pattern, meaning that the carbon in the sample is not well crystallized. The carbon-coated layer can only influence the surface of $LiMn_2O_4$ particles and almost has no effect on the bulk.

The morphologies and particle size of the prepared $LiMn_2O_4$ and $LiMn_2O_4$/C are examined by TEM, and the typical images of two samples are shown in Fig. 2. From Fig. 2a, c, we can see that the morphology of the particles is the polyhedral morphology, which indicates that the carbon layer had little difference to the particle morphology. In Fig. 2a, the average particle size is about 320–410 nm. The average particle size with 410–520 nm is a little larger in Fig. 2c. The HR-TEM image of a randomly selected single nanorod (Fig. 2b) indicates that the nanorod is structurally uniform and highly crystalline with lattice fringe extending to the grain boundary. As can be seen in Fig. 2d, the carbon-coated material shows an amorphous layer on the surface of $LiMn_2O_4$ core. The thickness of the carbon layer corresponds to around 2 nm. Because the carbon-coating layer is very thin, it is difficult to find any obvious differences between Fig. 3a, b.

The SEM images of the surface morphology of the bare $LiMn_2O_4$ and $LiMn_2O_4$/C powders are presented in Fig. 3. From Fig. 3, lots of small polyhedral particles are received, which indicates the shape of the spinel $LiMn_2O_4$. The two samples are homogeneously distributed with an average particle diameter of 5 μm, which suggests that the carbon layer has no obvious effect on the particle size. Besides, in Fig. 3a, b, no large difference can be observed from the SEM images. The narrow size distribution and unique morphology make the materials possible to achieve better electrochemical performances.

Figure 4 shows the initial discharge curves of the two samples at the rate of 0.1 C, and its electrochemical performance with respect to Li intercalation–deintercalation is investigated in the voltage range of 3.0–4.3 V. The discharge curves show the pseudo-plateaus at around 4.0 V, which is a typical profile for the electrochemical deinsertion/insertion of Li^+ from/into the $LiMn_2O_4$. At the same

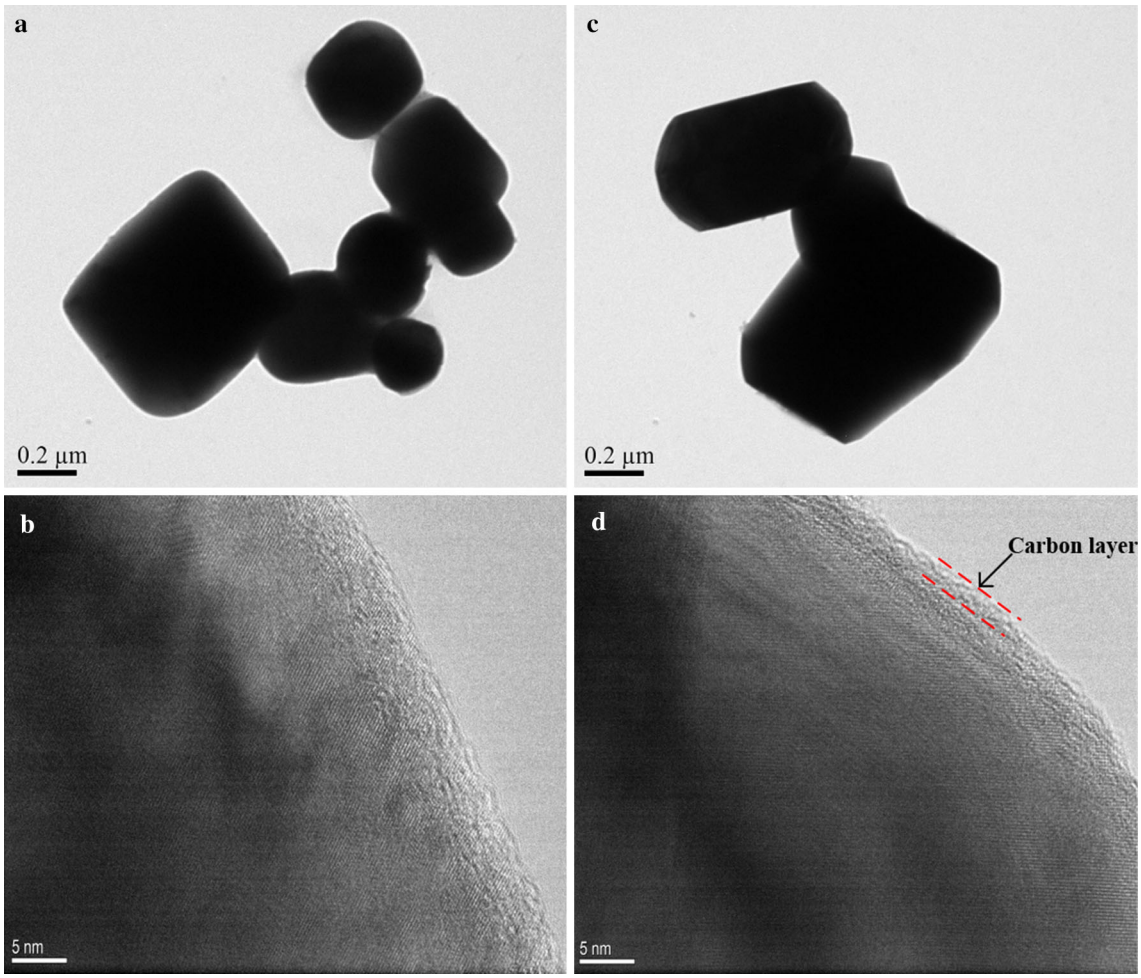

Fig. 2 **a** TEM and **b** HR-TEM images of $LiMn_2O_4$, **c** TEM and **d** HR-TEM images of $LiMn_2O_4$/C

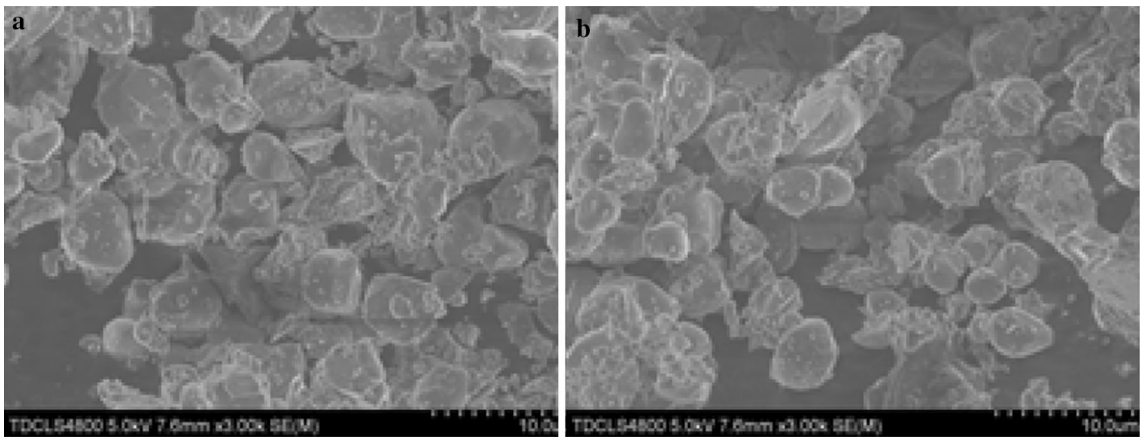

Fig. 3 SEM image of $LiMn_2O_4$ and $LiMn_2O_4$/C

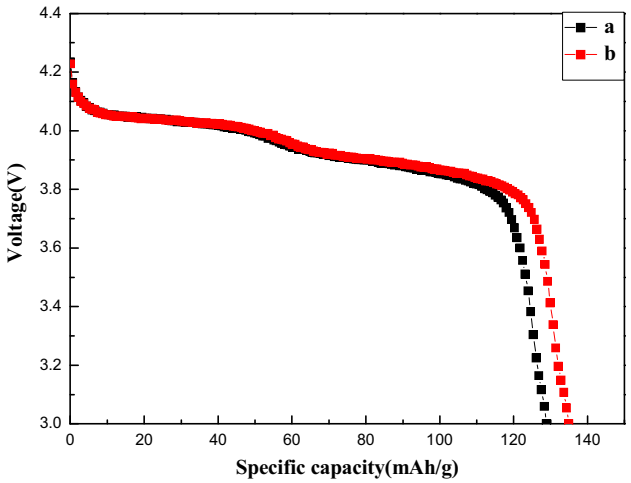

Fig. 4 Initial discharge curves of $LiMn_2O_4$ and $LiMn_2O_4$/C in the voltage of 3.0–4.3 V at room temperature

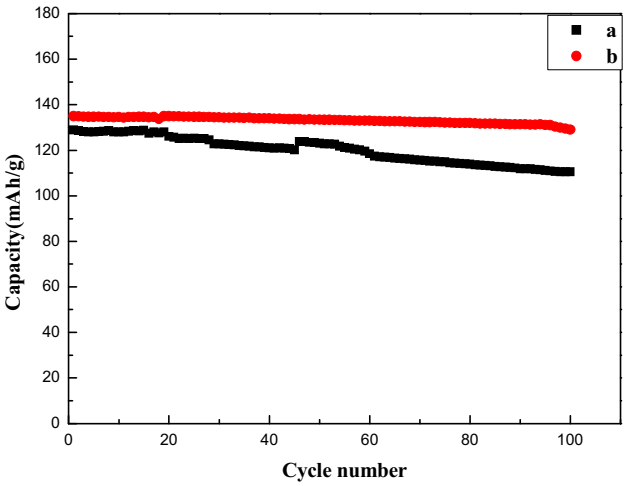

Fig. 5 Cycling performance of $LiMn_2O_4$ and $LiMn_2O_4$/C in the voltage of 3.0–4.3 V at room temperature

time, it is clearly seen that the $LiMn_2O_4$/C displays a much higher capacity than the pristine $LiMn_2O_4$. The initial discharge capacity for the $LiMn_2O_4$ microspheres (Fig. 4a) is 128.9 mAh g^{-1}, while that of the $LiMn_2O_4$/C microspheres (Fig. 4b) is 134.9 mAh g^{-1}. Sample (b), however, displays higher discharge capacity than that of sample (a) when cycles at the same current density. A slight increasing of capacity of sample (b) may contribute to the Li^+–Li^+ coulomb repulsion which is lower at the surface of carbon-coating material, thus enhancing local capacity as there on neighboring Li^+ outside the particle. Consequently, it can be concluded that the carbon layer forms a continuous conductive layer to enhance the electrochemical performance.

The modification effect on the capacity retention of the pristine $LiMn_2O_4$ is investigated as a function of the carbon layer. Figure 5 shows the cycling performances of the pristine $LiMn_2O_4$ and $LiMn_2O_4$/C at room temperature using Li metal as the counter electrode. From Fig. 5, it can be seen that sample (a) shows an average capacity loss of 0.146 mAh g^{-1} per cycle, in other words, after 100 charge/discharge cycles, with capacity losses of 14.20 %. However, in the case of the carbon layer, not only the initial capacity becomes higher, but also the discharge capacity after 100th cycles decreases to 129.1 mAh g^{-1} with the capacity losses of 4.3 %. The carbon layer is apparently the most effective in improving the cycling performance of $LiMn_2O_4$. The certain thickness of carbon layer can produce a long lithium diffusion length, which all can influence the deintercalation–intercalation of the lithium ions and restrict the cycling stability performance and capacity. Therefore, the cycling performance and specific capacity are enhanced due to the carbon layer which can avoid the core material directing contact with the acidic electrolyte; at the same time, it can improve the electronic conductivity of $LiMn_2O_4$ sample.

Nyquist plots of the sample $LiMn_2O_4$ (a) and $LiMn_2O_4$/C (b) using Li metal as the counter electrode are shown in Fig. 6. It could be seen that all two cells have a similar ohmic resistance, but the charge-transfer resistance (R_{ct}) of the sample $LiMn_2O_4$ was bigger ($R_{ct} \approx 201.6\ \Omega$) than the sample $LiMn_2O_4$/C ($R_{ct} \approx 109.3\ \Omega$). It could be seen clearly that the charge-transfer resistance (R_{ct}) of the $LiMn_2O_4$/C was much lower than that of the pristine one, which indicated that the rate capability of the sample $LiMn_2O_4$/C would be better than that of the pristine one. The dates of Nyquist plots indicate that the carbon coating can improve the conductivity of the material.

The discharge capacities of $LiMn_2O_4$ and $LiMn_2O_4$/C at different rates, varying from 0.1 to 1 C, using Li metal as the counter electrode are shown in Fig. 7a. The first specific discharge capacity of the bare $LiMn_2O_4$ (a) and $LiMn_2O_4$/C (b) is 128.4 mAh g^{-1} and 134.6 mAh g^{-1} at 0.1 C after 15 cycles. But the $LiMn_2O_4$/C keeps 97.18 % of its capacity compared with that at 0.1 C, which is larger than the pristine $LiMn_2O_4$ even at 1 C. Compared with the low rate, the specific capacities of the pristine are 120.1, 112.4, 98.3 mAh g^{-1}, and their capacity retentions are 96.42, 94.84, 91.66 % at 0.2 C, 0.5 C, 1 C after 15 cycles, respectively. As expected, the discharge capacity decreases with an increase in the rate. The figures show that even though the $LiMn_2O_4$ sample has uniform particle size particles, it displays inferior rate performances attributing to the large Mn dissolution from spinel material into the electrolyte. Simultaneously, the sample exhibits excellent low-rate performance, which demonstrates the acetone hydrothermal method is a powerful novel method to synthesize pure $LiMn_2O_4$ product. Whereas the $LiMn_2O_4$/C sample shows a faster increase in capacity than pure $LiMn_2O_4$, the reversible capacities of the $LiMn_2O_4$/C are 133.5, 132.7, 131.1 mAh g^{-1}, at 0.2 C, 0.5 C and 1 C after 15 cycles, corresponding to 1.80, 2.34 and 2.90 % capacity fading, respectively. The discharge capacities of $LiMn_2O_4$ and $LiMn_2O_4$/C at 2 and 5 C rates, using Li metal as the counter electrode, are shown in Fig. 7b. The specific capacities of the pristine are 105.1, 92.5 mAh g^{-1}, and their capacity retentions are 92.48, 89.51 % after ten cycles, respectively. Whereas we can clearly see that the $LiMn_2O_4$/C sample shows a faster increase in capacity than pure $LiMn_2O_4$, the reversible capacities of the $LiMn_2O_4$/C are 119.6, 112.8 mAh g^{-1} at 2 and 5 C after ten cycles, corresponding to 1.92 and 3.19 % capacity fading, respectively, which indicates the $LiMn_2O_4$/C has the excellent rate capacity.

The improvement of the electrochemical performance attributes to the existence of carbon layer which can reduce the Mn dissolution from bare $LiMn_2O_4$ into the electrolyte and provides intergrain connectivity to the hybrid

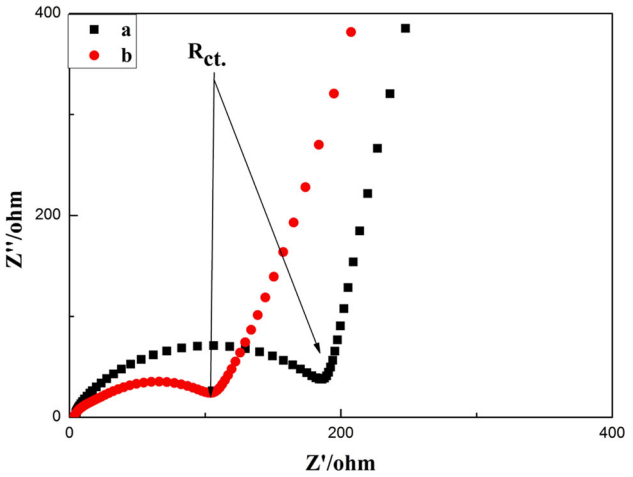

Fig. 6 Nyquist plots of $LiMn_2O_4$ (**a**) and $LiMn_2O_4$/C (**b**) using Li metal as the counter electrode

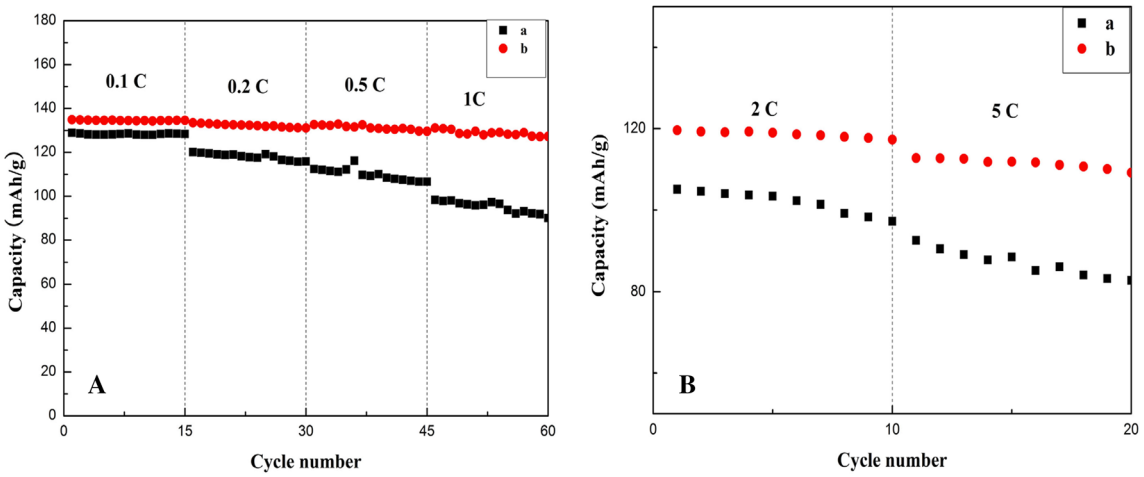

Fig. 7 Variation in discharge capacity versus cycle number for the $LiMn_2O_4$ (**a**) and $LiMn_2O_4$/C (**b**) at different rates using Li metal as the counter electrode, between 3.0 and 4.3 V

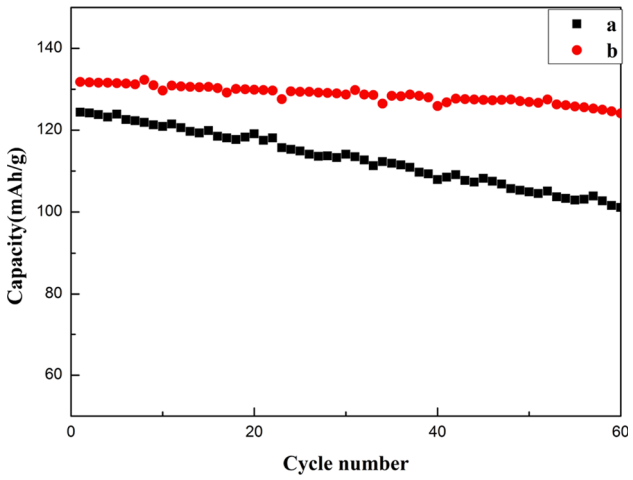

Fig. 8 Cycle performance of the $LiMn_2O_4$ (**a**) and $LiMn_2O_4$/C (**b**) at 55 °C at the rate of 0.1 C in the voltage range of 3.0–4.3 V

electrode. Evidently, the excellent rate capacity is due to the carbon layer on the surface of the bare $LiMn_2O_4$. The low-temperature, soft-chemistry and carbon-coated method discussed in this report, and we provide a promising way to synthesize spinel $LiMn_2O_4$ and $LiMn_2O_4$/C, which is vital for future EV application.

The cycle performance of the $LiMn_2O_4$ (a) and $LiMn_2O_4$/C (b) at the rate of 0.1 C at 55 °C is shown in Fig. 8. The pristine material exhibits a discharge capacity decline from 124.4 to 101.1 mAh g^{-1}, with a capacity loss of 18.73 % at the 60th cycle, whereas the sample $LiMn_2O_4$/C shows only 5.84 % discharge capacity loss. Therefore, the sample $LiMn_2O_4$/C exhibits more stable cycle performance than the pristine $LiMn_2O_4$.

4 Conclusion

In the present work, the structure and electrochemical properties of spinel $LiMn_2O_4$ synthesized by a novel acetone hydrothermal method are studied. Compared with the pristine $LiMn_2O_4$, the $LiMn_2O_4$/C shows much better capacity performance. The initial discharge capacity of $LiMn_2O_4$ is 128.9 mAh g^{-1} at 0.1 C rate, and the discharge capacity of the $LiMn_2O_4$/C increases to 134.9 mAh g^{-1} at 0.1 C rate. At the same time, it exhibits an excellent cycling reversibility after 100 cycles, and 95.7 % of discharge capacity can be retained. The $LiMn_2O_4$/C sample with excellent rate performance shows a faster increase in capacity than pure $LiMn_2O_4$, and the reversible capacities of the $LiMn_2O_4$/C are 133.5, 132.7, 131.1 mAh g^{-1} at 0.2 C, 0.5 C and 1 C. Even at higher rate (i.e., 2 C, 5 C), the reversible capacities of the $LiMn_2O_4$/C are 119.6, 112.8 mAh g^{-1} at 2 and 5 C after ten cycles, corresponding to 1.92 and 3.19 % capacity fading, respectively, which indicates the $LiMn_2O_4$/C has the excellent rate capacity. The spinel $LiMn_2O_4$ synthesized with this method is expected to present applications in lithium-ion batteries. Furthermore, the methodology with a low temperature and no sintering presents a new possibility to develop other cathode materials with excellent electrochemical performances.

Acknowledgments This work was partially supported by the National Natural Science Foundation of China (Nos. 20973124 and 21276185).

References

1. A.B. Eftekhari, B. Moghaddam, F. Yazdani, Moztarzadeh. Electrochim. Acta **52**, 1491 (2006)
2. D. Im, A.J. Manthiram, J. Electrochem. Soc. **150**, A742 (2003)
3. J.B. Goodenough, Solid State Ion. **69**, 184 (1994)
4. J.Y. Luo, Y.Y. Xia, Adv. Funct. Mater. **17**, 3877 (2007)
5. R.K. Katiyar, R. Singhal, K. Asmar, R. Valentin, R.S. Katiyar, J. Power Sources **194**, 526 (2009)
6. X.Q. Li, Z.X. Wang, R.F. Liang, H.J. Guo, X.H. Li, Q.Y. Chen, Trans. Nonferr. Metal. Soc. **19**, 1494 (2009)
7. G. Amatucci, J.M. Tarascon, J. Electrochem. Soc. **149**, K31–K46 (2002)
8. J. Guan, M. Liu, Solid State Ion. **110**, 21–28 (1998)
9. J.M. Tarascon, D. Guyomard, Electrochem. Acta **38**, 1221 (1993)
10. C.H. Lu, S.K. Saha, Mater. Sci. Eng. B Solid **79**, 247–250 (2001)
11. X. Qiu, X. Sun, W. Shen, N. Chen, Solid State Ion. **93**, 335–339 (1997)
12. Y. Liang, S. Bao, B. He, W. Zhou, H. Li, J. Electrochim. Soc **152**, A2030 (2005)
13. J. Liddle, S.M. Collins, B.M. Bartlett, Energy Environ. Sci. **3**, 1339–1346 (2010)
14. C. Miao, P.F. Bai, Q.Q. Jiang, S.Q. Sun, J. Power Sources **246**, 232–238 (2014)
15. J.M. Tarascon, D. Guyomard, Electrochim. Acta **38**, 1221–1231 (1993)
16. K. Kanamura, H. Naito, T. Yao, Z. Takehara, J. Mater. Chem. **6**, 33 (1996)
17. K. Oikawa, T. Kamiyama, F. Izumi, B.C. Chakoumakos, H. Ikuta, M. Wakihara, J.Q. Li, Y. Matsui, Solid State Ion. **109**, 35 (1998)
18. M.Y. Song, D.S. Ahn, H.R. Park, J. Power Sources **83**, 57 (1999)
19. Y.K. Sun, Y.S. Jeon, H.J. Lee, Electrochem. Solid-State Lett. **3**, 7 (2000)
20. Q.Q. Jiang, X.Y. Wang, C. Miao, Z.Y. Tang, RSC Adv. **3**(30), 12088–12090 (2013)
21. R. Benedek, M.M. Thackeray, Electrochem. Solid-State Lett. **9**, A265 (2006)
22. B. Aurbach, G. Markovsky, E. Salitra, Y. Markevich, M. Talyossef, L. Koltypin, B. Nazar, D.Kovacheva Ellis, J. Power Sources **165**, 491 (2007)
23. N. Nakayama, T. Nozawa, Y. Iriyama, T. Abe, Z. Ogumi, K. Kikuchi, J. Power Sources **174**, 695 (2007)
24. C.Y. Ouyang, S.Q. Shi, M.S. Lei, J. Alloys Compd. **474**, 370 (2009)
25. Y.Y. Xia, T. Sakai, T. Fujieda, X.Q. Yang, X. Sun, Z.F. Ma, J. McBreen, M. Yoshio, J. Electrochem. Soc. **148**, A723 (2001)
26. Y. Shao-Horn, Y. Ein-Eli, A.D. Robertson, W.F. Averill, S.A. Hackney, W.F. Howard Jr, J. Electrochem. Soc. **145**, 16 (1998)